First average and local heat transfer measurements on a forced air-flow at low Re-numbers through a rectangular channel with ribbed surfaces

D. Fustinoni, P. Gramazio, L.P.M. Colombo, A. Niro[1]

Department of Energy, Politecnico di Milano Campus Bovisa,

via Lambruschini, 4 – I-20156 Milano, Italy

[1] Corresponding author: alfonso.niro@polimi.it

Abstract. In this paper we present new experimental results on average and local heat transfer characteristics of a forced air-flow through a rectangular channel with the lower and upper surfaces with continuous, square ribs. Comparisons with data inside a flat rectangular channel are also presented. The experimental duct cross-section is 120 mm wide and 12 mm height, and the channel is operated with the lower and upper walls at fixed temperature whereas the sides are adiabatic. Ribs are transverse to the flow or tilted with an angle of 45° or 60°; for the transverse configurations, three values of the pitch-to-heigth ratio *p/e*, namely 10, 20 or 40, are investigated. Reynolds numbers, based on the duct hydraulic diameter, are varied between 600 and 8000. Accordingly, the average Nusselt numbers and the Darcy-Weisbach friction factor are presented. In addition, first results on local temperature measurements by means of IR-thermography, obtained in a properly modified test section operated at a constant heat flux, are shown for the transverse- rib configuration with *p/e*=10 and *e*=4-mm.

1. Introduction

Heat transfer in forced convection inside rectangular channels is a very interesting matter for industry since it is encountered in critical heat transfer applications like gas-turbine blade cooling, as well as in devices largely used such as plate-fin compact heat exchangers. In designing these devices, high values of heat transfer area per unit volume are looked for; however, if this parameter is increased over a given value, thermal performances start worsening. In fact, the higher the surface-to-volume ratio the narrower the passages, so air velocity has to be lowered to maintain acceptable pressure drops; but narrow passages and low air velocities bring to a flow laminarization that is of course characterized by a quite poor convective coefficient which eventually defeats completely the benefits of area increase. To overcome this limit, heat transfer is enhanced by configuring surfaces with a large variety of fins and ribs, which are an efficient and cost-effective solution. The literature review shows that, starting from '70s, a continuously growing number of studies is concerned with heat transfer over surfaces roughened with square ribs, as this is a very attractive solution both for gas-turbine blade cooling and compact heat exchangers.

A crucial feature is the arrangement of the ribs with respect to the flow direction. The number of possible configurations, indeed, is very large but four arrangements have been particularly considered so far in literature, namely, with transverse-, parallel-tilted-, cross-inclined- and V-shaped-ribs; in ad-

dition, ribs may be assembled both in a staggered or in-line configuration. A brief discussion of relevant works in literature is presented below by using the following dimensionless geometric parameters: the channel aspect ratio *AR*, i.e, the ratio of the base to the height of the channel cross section, the dimensionless pitch *p/e* , i.e., the ratio of the pitch to the height of the rib, and the blockage factor e/D_h defined as the ratio of the rib height to the channel hydraulic diameter.

Transverse ribs. Early works were performed between the '70s and '80s by Burggraf [1] and Han et al. [2]-[4]. They investigated the effect of square ribs made of conductive material, arranged with constant pitch and blockage factor e/D_h ranging within 0.05 and 0.1. The results showed the existence of a maximum in both the average Nusselt number ($2< Nu/Nu_0< 3$) and the apparent friction factor ($f/f_0 \geq 20$) for $p/e = 10$. This was explained with the reattachment of the fluid vein between two consecutive ribs, which does not occur for lower p/e. On the other hand, for greater p/e the boundary layer growth downward the reattachment zone reduces the heat transfer coefficient.

Parallel-tilted ribs. The first major studies were conducted from the first half of the 80s by Han [5]-[10], Park [11] and Kukreja [12]. It was observed that inclination of the ribs with respect to the main direction of flow produces higher performance in terms of heat exchange due to the presence of secondary flows. Actually, the inclination creates two counter-rotating vortices developing near the rib and sliding along it. They interact with the main flow carrying part of the colder core towards the wall. Furthermore, the interaction between the main flow and secondary flows influences the recirculation zone between successive ribs, the reattachment of the flow and it inhibits the growth of the boundary layer downstream the vein reattachment. Particular attention was devoted to an inclination angle $\alpha = 45°$ and it was found that the optimum dimensionless pitch *p/e* strongly depends on both e/D_h and *AR*. The most studied configuration presents *AR*=1 with all the sides heated.

Cross-tilted- and V-shaped ribs. More recently, i.e., from the 90s, studies have been devoted to these configurations in order to enhance the effect of secondary flows, for example Han et al. [10], Krukeja et al. [12], Gao and Sunden [13]. In particular, V-shaped ribs may present the apex upward or downward the main flow direction. In the former arrangement, secondary flows move from the center to the lateral sides of the channel, whereas in the latter the situation is reversed. It has not been yet assessed which configuration is the best in enhancing heat transfer, because controversial results have been found, probably due to the different boundary conditions taken into consideration.

Finally, in the last decade rectangular channels with only one heated, ribbed surface have aroused great interest for applications in renewable energy technologies as solar air heaters. Reviews on this subject are reported in Bhushan and Singh [18] and Hans et al. [19].

A closer look reveals that most of the work done up to now focused on turbulent flow regimes. Moreover, two aspects are very little investigated, namely the impact of high values of the blockage factor, and the transition between laminar and turbulent regime. Both these aspects are very relevant in the design of compact heat exchangers, as well shown by the specific literature [20]. For this reason it has been started an experimental campaign aimed to investigate the characteristics of heat transfer coefficients and pressure drops in rectangular ducts with variously arranged square ribs, in a range of Reynolds numbers between 600 and 8000. In these conditions, it is possible to explore both the turbulence onset and the transition region. Local temperature measurements also allow to identify the flow structures promoted by the ribs. In this paper we present a selection of the available results while experimental runs are under completion.

2. Experimental setup

As schematically shown in figure 1, the experimental setup basically consists of the air-circuit containing the test section. As average heat transfer measurements are performed at fixed temperature whereas the local ones at constant heat flux, two different test sections with auxiliary systems are used. In the following, first we describe the air-circuit and then the two test sections.

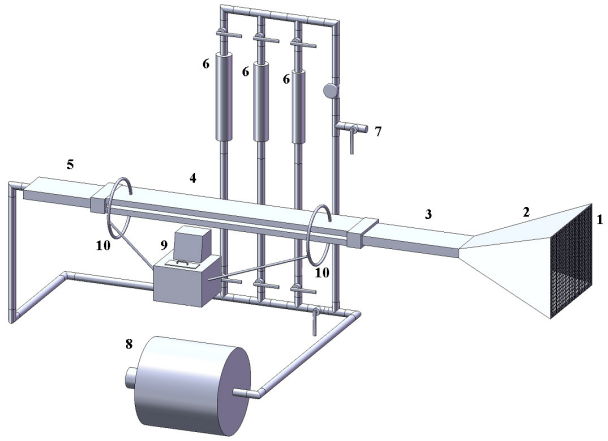

Figure 1. Schematics of the experimental setup with test section operated at fixed temperature: 1. fine mesh screen cover; 2. convergent air inlet; 3. entry-section; 4. test-section; 5. exit-section; 6. float-type flow-meters; 7. by-pass; 8. blower; 9. heat bath; 10. water circuit piping (only for the test section operating at uniform temperature.

Through a convergent, room air flows into the circuit; a fine mesh screen covers the convergent inlet whereas at its outlet there is a flow straightener. Inside the convergent a thermo-resistance is mounted to measure the air temperature. From the straightener, air flows into an entry-section that is a rectangular duct with the same cross dimensions as the tested channel; entry-section is near 40 times the channel hydraulic diameter, and its walls are made of plexiglass plates and are not heated. At the end of this section, air enters the test-section that is a 120-mm wide, 12-mm height, 880-mm long duct. At the test-section outlet, there is a short exit-section equipped with a mixing section in order to measure the air bulk temperature. Finally, the inlet and outlet of the test section are provided with pressure taps. Downstream the exit-section there are three float-type flow-meters, connected in parallel, with full scale of 6, 23.5 and 40 m^3/h respectively, a metering valve, and a 7-stage, 30 kPa-head, 5.5 kW-power blower operating in suction mode. The exhausted air is discharged outside the laboratory. Air temperature is also measured upstream the flow-meters by means of a thermocouple plugged in the pipe.
Test section operated at uniform temperature. The lower and upper walls are two aluminium plates of 10-mm minimum thickness; the backside of each plate is covered by a cap strongly tightened to the plate, so that they form a jacket where the heating water flows. To check if temperature is uniform over the heated walls, five thermocouples are embedded in the lower wall, and three in the upper one at the locations displayed in figure 2a. Finally, test-section sides are closed by 4-mm-thick glass slabs.

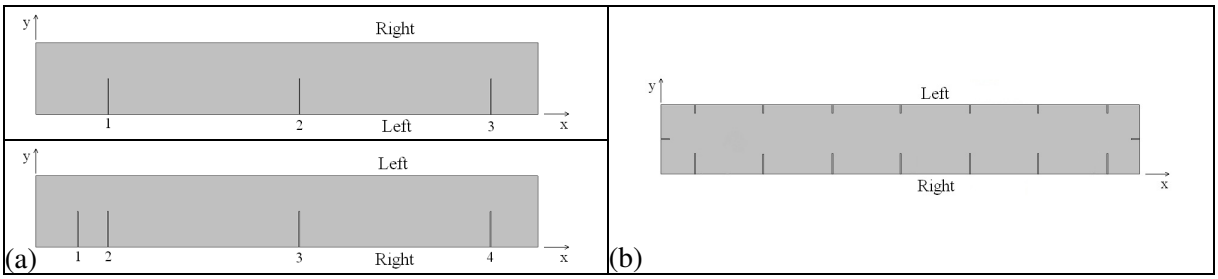

Figure 2. Thermocouples locations for the test channel operated (a) at uniform temperature, for the upper and lower walls respectively, and (b) at uniform heat flux (only lower wall).

The heating circuit is mainly composed by a heat bath which provides a high mass flow-rate of water at constant temperature, and by the channels built into the upper and lower test-section walls (water and air stream in counterflow); two thermocouples are placed inside each water channel, near the inlet and outlet ports, respectively. The heat bath is the ThermoHaake B12 with a tank of 12-dm^3, a 3-kW heater and a high precision controller; water temperature inside the tank is kept constant within 0.01K.
Test section operated at uniform heat flux. Local heat transfer measurements by IR-thermography can not be performed while keeping the wall at uniform temperature and without providing to the IR-

camera an optical access to the duct interior. Consequently, the test section was properly modified by operating the lower wall at fixed heat flux while mounting into the upper one a 120 mm x 80 mm, germanium window, with the longer side in the streamwise direction (as known, germanium is a highly transparent material to the near infrared radiation, in fact its total transmissivity is equal to 0.95 within the range from 3 to 5 μm). In order to make easier positioning the germanium window along the test section, and more uniform thermal boundary condition on the upper wall, this is insulated and not heated. On the other hand, it is well known that heat transfer coefficient in turbulent forced convection inside a duct is independent to a large extent of thermal boundary conditions; in any case, we designed the lower wall in order to limit the temperature differences along it within about 10 K. Hence, the lower wall is made of a 3 mm thick, 120 mm wide, 800 mm long, AISI 316 stainless steel plate. The measurement side is blackened, whilst a thin foil heater is stuck on the opposite side. Sixteen thermocouples are embedded in the plate back side and their locations are shown in figure 2b.

3. Measurements, data processing and error analysis

In this section we describe the measurements carried out along with calibrations and error analysis.

3.1. Calibration

The thermocouples used are T-type with 0.5-mm-diameter wires, whereas the thermo-resistances are 4-wires, 100-ohm, Platinum type, i.e., PT100, with dimensions of 2 mm x 4 mm. Both thermocouples and thermo-resistances were all preliminary calibrated over five points within the temperature range from 22 to 60 °C, by means of the ThermoHaake heat bath. The probes were immersed all together into the bath; for each calibration point, 160 readings per probe were collected; the resulting standard deviation is of 0.02 K for the thermocouples, and of 0.01 K for the thermo-resistances. All temperature measurements are performed by means of an Agilent 34970A data logger equipped with a relay multiplexer and a 6½ digit multimeter. The channels are sequentially read, by waiting a 0.5-s settling time after each channel-locking, with an integration time of 400 ms which ensures a standard deviation of 0.01 K that is less than or equal to the probe uncertainties; consequently, reading cycles are performed every 20 s. Pressure drops are measured by connecting the two pressure taps to a differential micromanometer with a full scale of 250 Pa and a 0.125-Pa sensitivity. Air volume-flow-rate is measured by means of the aforementioned float-type flow meters which have a 2% nominal accuracy; however, by means of a calibration performed by measuring pressure drops of laminar air-flows through a smooth circular tube, we found that their accuracy is better of 1%. IR-camera was preliminary calibrated by shooting through the germanium window a surface with the same finishing as the test section and kept at uniform and constant temperature. Within the operating range, the camera sensitivity is at least of 0.09 K.

3.2. Average measurements

A properly defined test procedure is adopted in order to attain regime conditions with all temperature time-fluctuations within a 0.02-K band, and a channel wall-temperature uniformity within 0.1 K over the entire heated length. Based on a standard deviation analysis, single measurement results by averaging 20 reading-cycles. The apparent Darcy friction factor and the average Nusselt number over the entire test section are calculated as follows

$$f = \frac{2\Delta p A^2 D_h}{\rho \dot{V}^2 \ell_{taps}} \tag{1}$$

$$Nu = \frac{D_h}{k} \frac{\rho \dot{V} c_P}{A_{S,T}} \ln \frac{\theta_i}{\theta_o} \tag{2}$$

$$Nu = \frac{D_h}{k} \frac{\rho \dot{V} c_P \left(T_o - T_i\right)}{A_{S,H} \left[T_w - \left(T_o + T_i\right)/2\right]} \tag{3}$$

where Equations 2 and 3 are used for the tests at fixed temperature and uniform heat flux, respectively, $\dot{V}$ the air volume-flow-rate, ρ the density calculated at the temperature where $\dot{V}$ is measured, D_h the

hydraulic diameter, Δp the pressure drop, ℓ_{taps} the distance between the pressure taps, A the maximum cross section area, A_S the net total heated area, c_P the specific heat at constant pressure, k the thermal conductivity, T_i and T_o the bulk temperatures at the test section inlet and outlet respectively, θ_i and θ_o the corresponding wall-to-bulk-temperature differences, T_w the average wall temperature along the thermally developed region evaluated by the thermocouple measurements. The error analysis performed according to Moffat [21] gives an uncertainty less than 3% on the convective coefficient for both the tested thermal boundary conditions, and less than 7% on the apparent Darcy friction factor.

3.3. Local temperature measurements

Local temperature distribution is measured by the Raytheon Radiance HS IR-camera, with a 25-mK sensitivity, InSb Focal Plane Array detector; the acquisition rate is of 140 fps at full resolution, i.e., 256×256 pixels. As thermal images are affected by noise, a sequence of 700 images is recorded and then they are averaged pixel by pixel; the resulting field of time-averaged temperatures is characterized by a mean standard deviation of 0.09 K, namely, equal to the IR-camera sensitivity. Notwithstanding the care devoted in reducing thermal dispersions, spanwise temperature distribution tends to lower slightly at the borders, i.e., next to the channel vertical walls. Thus, we decided to cut the pixel rows falling within a 20-mm band both from the top and the bottom of the thermographic images; as a consequence, the observation region becomes 40-mm wide in the spanwise direction. In spite of the time-averaging filtering, the resulting temperature distribution is still affected by high frequency disturbance, and hence we decided to average temperature along y-direction, being the time-mean temperature field essentially 1-D in the observation region. The result is a smooth distribution of temperature along the flow direction.

4. Results and discussion

In order to assess the experimental procedures, heat transfer coefficients and pressure drops were measured in a reference configuration, i.e., a flat rectangular channel. In figure 3 the average Nusselt number is plotted versus the Reynolds number; the graph reports the values for both kinds of the tested thermal boundary conditions, namely, fixed temperature and fixed heat flux, the latter only for the turbulent regime. Finally, the trends calculated with the correlations of Shah and London and of Gnielinsky are also plotted in the graph. As it can be seen, the agreement between experimental and expected values is very good, and there are not appreciable differences between data obtained with the two different test sections. Figure 4 shows the experimental values of the apparent Darcy-Weisebach friction factor plotted versus the Reynolds number; also in this case, there is a very satisfactory agreement with the values estimated by the Shah and London correlations.

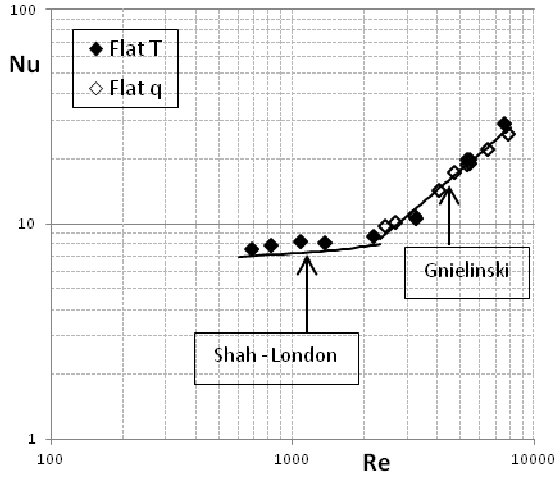

Figure 3. Average Nusselt number vs Reynolds number inside flat rectangular channel.

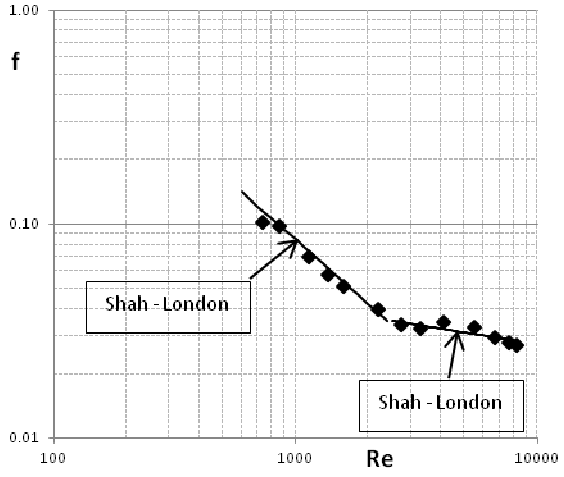

Figure 4. Darcy-Weisebach friction factor vs Reynolds number inside flat rectangular channel.

Table 1. Configurations experimentally studied.

	90°	60°	45°
Staggered	p/e = 10, 20, 40 e = 2, 4 mm	p/e = 10 e = 4 mm	p/e = 10 e = 4 mm
In-line	p/e = 10 and e = 4 mm	p/e = 10 and e = 4 mm	p/e = 10 and e = 4 mm

Table 1 lists the configurations experimentally studied here presented. Figure 5 reports the Darcy-Weisebach friction factor plotted versus the Reynolds number for all the configurations with staggered transverse ribs; data for the flat channel are also plotted for comparison. These data display the typical trend of flows through a duct with walls characterized by an equivalent sand roughness, namely, the friction factor becomes independent of Re for sufficiently high values. It is noteworthy that at the highest of the two blockage values, corresponding to a rib height of 4 mm, the flow appears to be turbulent at any Re; conversely, at the lowest blockage, this behaviour occurs only for *p/e*=10 while the turbulence onset shifting to higher Re as the dimensionless pitch increases. Figure 6 shows the values of the friction factor plotted versus the Reynolds number for configurations with tilted ribs at different angles and arrangements but with *p/e*=10 and *e*=4 mm. The friction factor appears to be almost independent of Re, probably due to the high value of blockage as already observed for the transverse configuration but, for low Re values, staggered and in-line configurations display opposite trends.

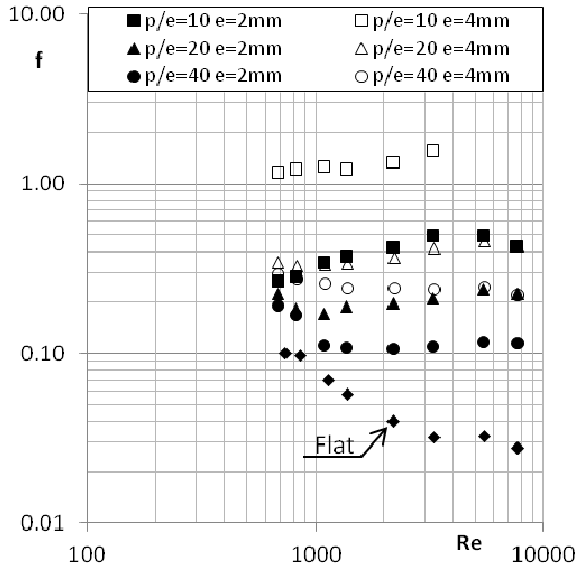

Figure 5. Friction factor vs Reynolds number for transverse-ribs in staggered arrangements at different values of dimensionless pitch and height.

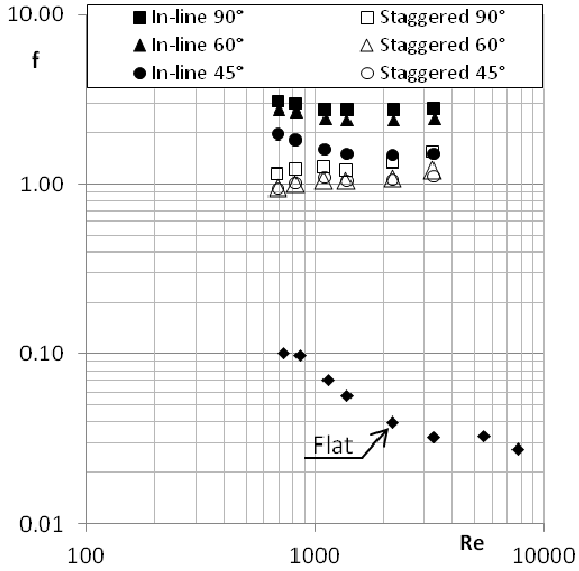

Figure 6. Friction factor vs Reynolds number for different rib tilting angles and arrangements for dimensionless pitch *p/e*=10 and height *e*=4mm.

Figure 7 shows the experimental values of the average Nusselt number plotted versus the Reynolds number for the same configurations considered in figure 5, included the reference case with flat walls. As it can be seen, these results are in good agreement with friction data, namely, flow seems to become turbulent at lower Re either for increasing blockage or decreasing dimensionless pitch. In turbulent regime, Nusselt number displays a power law dependence on Re with the same exponent as in the flat channel, i.e., about 0.8, but with a larger multiplying constant. The enhancement factor ranges between about 1.0 and 4.0 for the lowest of the two blockage values, and from 1.2 and 4.7 for the highest one; however its trend is generally not monotonic with Re but in some cases it shows a maximum; further investigation would be needed to assess whether there exists an optimum for any configuration. Figure 8 shows the experimental values of the average Nusselt number plotted versus the Reynolds number for the configurations with tilted ribs. It can be observed that values differ at most 15% from

each other; however, for the staggered arrangements, the Nusselt number is always larger, and the highest values are found for 45°-tilted-ribs just as reported in literature. Furthermore, the latter is also the best performing configuration of the in-line arrangements; in particular, up to about Re=1000, Nu values are practically the same as for the corresponding staggered arrangement, whereas for higher Re they lower about 7%. However, caution has to be used in drawing conclusions from this trend as this difference is of the same magnitude of the experimental error. On the whole, the enhancement factor ranges between about 1.2 and 5.1. These data do not allow more specific considerations about the influence of the tilting angle on heat transfer characteristics.
Finally, figure 9 shows the temperature field over a 120-mm long, 40-mm wide region of the heated wall with transverse ribs; the trailing edge of the observed region is at 250 mm from the channel exit. Figure 10 displays the streamwise temperature distribution, obtained by averaging along the y-direction the time-mean temperature field. As it can be seen, temperature distribution clearly highlights the

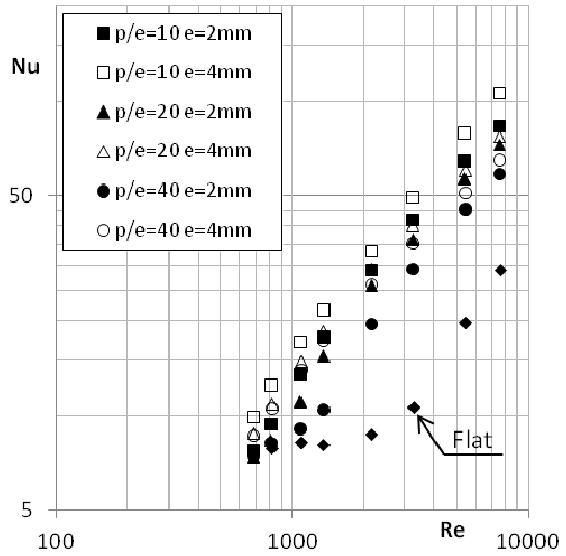

Figure 7. Average Nusselt number vs Reynolds number for staggered transverse-ribs at different values of dimensionless pitch and height.

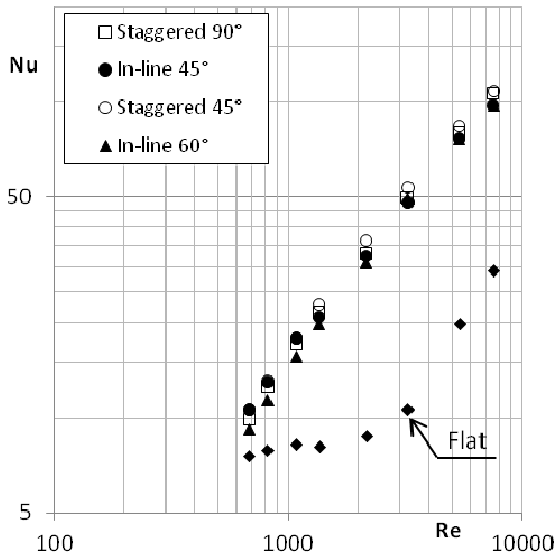

Figure 8. Average Nusselt number vs Reynolds number for different rib tilting angles and arrangements with *p/e*=10 and *e*=4mm.

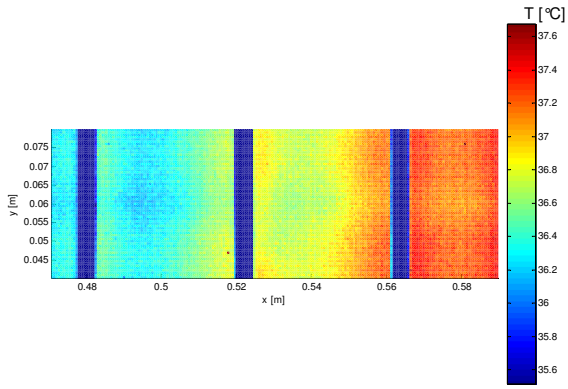

Figure 9. Time-mean wall temperature field at Re=5400 for the transverse-rib configuration with *p/e*=10 and *e*=4-mm.

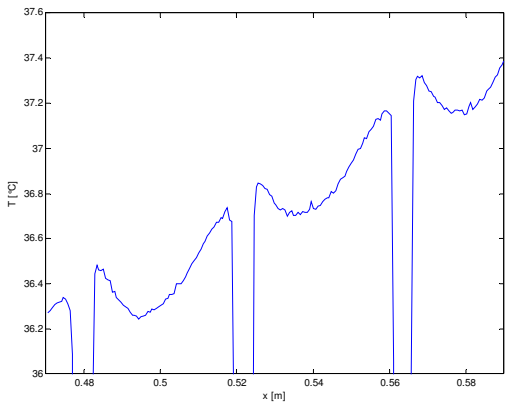

Figure 10. Streamwise distribution of the y-averaged temperature from the time-mean wall temperature field of figure 9.

rib effect on fluid-dynamics and heat transfer. Particularly, for the case reported here, the temperature shows a minimum at near one third of pitch downstream any ribs; of course, at same locations, heat transfer coefficient, not shown, has a maximum provided that a linear increase of air bulk temperature along the channel is assumed. In any case, differences of the convective coefficient are not large being within 6%.

5. Conclusions

In the investigated range of Reynolds numbers (600 – 8000), rib-roughened surfaces proved to enhance significantly heat transfer within rectangular channels, though increasing pressure drop as well. From the collected data, general conclusions can be drawn making a distinction between transverse and tilted rib arrangements, as follows.

Transverse and staggered ribs:

- the friction factor becomes nearly independent of Re by either increasing blockage or decreasing the dimensionless pitch; hence, turbulence seems to onset at Re even lower than 1000;
- the Nusselt number in such conditions shows a power law dependence on the Reynolds number with 0.8 exponent, i.e, a typical value for turbulent flow;
- the highest heat transfer enhancement factor is 4.7 and it seems to be related to an optimal dimensionless pitch.

Tilted ribs:

- the friction factor shows a weak dependence on the Reynolds number only for Re<1000, decreasing for staggered ribs, whereas increasing for in-line ribs;
- the Nusselt number for staggered arrangements is slightly larger than for in-line ones;
- 45°-tilted ribs reach the best heat transfer performance: the staggered arrangement shows the highest enhancement factor equal to 5.1.

Local temperature measurements are useful to investigate enhancement mechanisms; specifically, the heated wall temperature reaches a minimum downstream each rib, at near one third pitch for the tested configuration, and hence the heat transfer coefficient periodically attains a maximum.

6. References

[1] Burggraf F 1970 *ASME* (New York) 70-79
[2] Han J C, Glicksman L R and Rohsenow W M 1978 *J. Heat Trans.* **21** 1143-56
[3] Han J C and Lei C K 1983 *ASME*
[4] Han J C 1984 *J. Heat Trans.* **106** 774-781
[5] Han J C and Park J S 1985 *J. Eng. Gas Turb. Power* **107** 628-635
[6] Han J C 1988 Heat *ASME J. Heat Trans.* **110** 321-328
[7] Han J C and Park J S 1988 *Int. J. Heat Mass Tran.* **31** 183-195
[8] Han J C, Ou S, Park J S and Lei C K 1989 *Int. J. Heat Mass Tran.* **32** 1619-30
[9] Han J C and Zhang Y M 1991 *J. Turbomach.* **113** 123-130
[10] Han J C, Zhang Y M and Lee C P 1991 *J. Heat Trans.* **113** 590-596
[11] Park J S, Han J C, Huang Y, Ou S and Boyle R J 1992 *Int. J. Heat Mass Tran.* **35** 2891-903
[12] Kukreja R T, Lau S C and McMillin R D 1993 *Int. J. Heat Mass Tran.* **36** 2013-20
[13] Gao X and Sunden B 2001 *Exp. Therm. Fluid Sci.* **24** 25-34
[14] Han J C and Zhang Y M 1992 *Int. J. Heat Mass Tran.* **35** 513-523
[15] Liu T M, Chen C C and Tsai T W 2000 *J. Heat Trans.* **122** 327-335
[16] Cavallero D and Tanda G 2002 *Exp. Therm. Fluid Sci.* **26** 115-121
[17] Tanda G 2004 *Int. J. Heat Mass Tran.* **47** 229-243
[18] Bhushan B and Singh R 2010 *Energy* **35** 202-212
[19] Hans V S, Saini R P and Saini J S 2010 *Sol. Energy* **84** 898-91
[20] Webb R L 1994 *Principles of enhanced heat transfer* (New York: Winley-Interscience)
[21] Moffat R J 1988 Describing the uncertainties in experimental results *Exp. Therm. Fluid Sci.***1** 3-17